POLITECNICO DI TORINO
Repository ISTITUZIONALE

Sensitivity analysis for the design optimisation of an energy tunnel based hydronic heated pavement

Original
Sensitivity analysis for the design optimisation of an energy tunnel based hydronic heated pavement / De Feudis, S., Insana, A., Barla, M.. - In: TRANSPORTATION GEOTECHNICS. - ISSN 2214-3912. - 56:(2026), pp. 1-16. [10.1016/j.trgeo.2025.101692]

Availability:
This version is available at: 11583/3004088 since: 2025-10-16T07:18:48Z

Publisher:
Elsevier

Published
DOI:10.1016/j.trgeo.2025.101692

Terms of use:

This article is made available under terms and conditions as specified in the corresponding bibliographic description in the repository

Publisher copyright

(Article begins on next page)

24 June 2026

Transportation Geotechnics 56 (2026) 101692

Contents lists available at ScienceDirect

Transportation Geotechnics

journal homepage: www.elsevier.com/locate/trgeo

Sensitivity analysis for the design optimisation of an energy tunnel based hydronic heated pavement

S. De Feudis *, A. Insana, M. Barla

Department of Structural, Building and Geotechnical Engineering, Politecnico di Torino, Turin, Italy

ARTICLE INFO

Keywords:
Anti-icing
Road safety
Hydronic heated pavement
Geothermal energy
Environmental sustainability

ABSTRACT

To cope with road safety management during cold seasons, chemical agents such as sodium, magnesium and calcium chlorides are usually chosen for their effectiveness and rapidity of action. However, besides accelerating road pavement degradation, these may also induce several environmental damages, such as altering the chemical composition of aquifers. For this reason, electric- or hydronic-based solutions have been explored, developed and tested successfully. The paper investigates the performance of a hydronic heated pavement supplied by an energy tunnel as a function of geometrical, operational and environmental factors. Thermo-hydraulic numerical analyses are adopted to guide the realisation of a full-scale prototype of an anti-icing system in an existing tunnel in the North-West of Italy. An economic assessment is then presented.

Introduction

Hoar frost formation and snow accumulation on road pavements pose noteworthy issues threatening drivers' safety. It is worth noticing that the friction between the asphalt and the tyres reduces by around 80 % when the road surface is frozen or snow-covered. The most common response to this problem is embodied by chemical agents, such as sodium (NaCl), magnesium ($MgCl_2$) and calcium ($CaCl_2$) chlorides, able to lower the freezing temperature of water up to −10.0 °C, −15.0 °C and −25.0 °C, respectively [1]. While the former can serve as both a preventive and a corrective solution, the latter are used solely to melt ice and snow once developed due to their tendency to create a slippery coating on asphalt-paved surfaces under certain humidity conditions [2].

Despite their effectiveness and rapidity of action, the use of chemical agents leads to a remarkable maintenance need and, above all, environmental issues. On the one hand, indeed, the de-icing salts have detrimental impacts on infrastructures, inducing corrosion of steel rebars and weakening of cement pastes in concrete structures [3], and degrading the mechanical performance and the durability of asphalt pavements [4–7]. On the other hand, these may leak into the ground, provoking substantial damage to the vegetation [8] and rivers, lakes and aquifers that experience an increment of pH and, thus, a reduction in the quality of freshwater [9,10]. The hidden costs related to these issues were quantified by Dindorf et al. [11] for the Minnesota Pollution Control Agency to range approximately between $280.00 million and $1.17 billion. It is worth noticing that the sole extra road maintenance was assessed at $600.00 per ton of salt used.

For the reasons stated above, new alternatives have been recently tested and developed, such as approaches based on agricultural bio-products [9] or electric resistance [12,13] and hydronic heating by, for instance, gas boilers [14] or solar collectors [15]. With particular reference to the latter, the possibility of heating the thermal fluid through shallow geothermal systems (often incorporating ground source heat pumps) has also been investigated, demonstrating the validity and reliability of the approach.

Eugster & Schatzmann [16] and Eugster [8] documented one of the earliest projects of this kind: the SERSO pilot plant in Switzerland. This comprises ninety-one 65.0 m long borehole heat exchangers serving over 1300.0 m^2 of a bridge deck. The system aims at preventing ice formation on the road surface by taking advantage of the solar thermal energy stored within 55000.0 m^3 of rock mass during the summer season. The SERSO system was tested to deliver a typical heat output of 100.0 W/m^2 and maintain the pavement temperature above 0.0 °C throughout the 1000.0 h winter operativity.

Similar systems were also implemented in Aomori and Aizu-Bange, Japan and chronicled by Morita & Tago [17] and Islam et al. [18], respectively. The GAIA snow-melting system reaps the benefits of a geothermal system composed of four 151.4 m deep downhole coaxial heat exchangers and a heat pump to supply a design thermal output of

* Corresponding author.
E-mail address: simone.defeudis@polito.it (S. De Feudis).

https://doi.org/10.1016/j.trgeo.2025.101692
Received 9 May 2025; Received in revised form 14 August 2025; Accepted 22 August 2025
Available online 24 August 2025
2214-3912/© 2025 The Authors. Published by Elsevier Ltd. This is an open access article under the CC BY-NC-ND license (http://creativecommons.org/licenses/by-nc-nd/4.0/).

about 170.0 W/m^2. In the Nanaori-Toge tunnel, instead, a free-heating system was realised. This takes advantage of 1000.0 m long horizontal heat exchangers placed 1.0 m deep within the road pavement to anti-ice 175.0 m^2 of road pavement at the tunnel portal, delivering a measured heat flux ranging from 25.0 W/m^2 to 175.0 W/m^2 throughout a 50-day operational test. Also in Western Japan, Yoshitake et al. [19] developed a hydronic system employing a buried tank enclosing groundwater at 1.0 °C to 12.0 °C based on the season and the operativity.

To address more recent applications and testbeds, Barbagallo [20] describes a hybrid technology that employs an open-loop geothermal system aided by electric and oil-fired boilers to heat thirty-five hydronic heated aircraft parking stands of 600.0–700.0 m^2 each of the Gardermoen International Airport in Norway. This technology was found to be effective up to an external air temperature of −8.0 °C. A similar system is also implemented at the Arlanda International Airport, Sweden. Johnsson & Adl-Zarrabi [21,22] discussed another Nordic case study in Östersund, Sweden. The testbed is constituted by a 70.0 m^2 concrete pavement heated with four borehole heat exchangers, analogous to the SERSO system. Unlike the other implementations, which aim at maintaining the temperature of the pavement above 0.0 °C, in this case, a control strategy as a function of the dew-point temperature was developed. Such a strategy is more efficient since, actually, hoar frost forms when the road temperature falls below a sub-zero dew-point temperature. This, in turn, depends on air humidity: the lesser it is, the lower the air temperature needed to develop hoar frost [23]. Instead, Habibzadeh-Bigdarvish et al. [24] tested a novel external heating system on a full scale. This is installed beneath the bridge decks and insulated from the external environment through spray foam. With the aid of a ground source heat pump, heat fluxes of 433.4 W/m^2 and 236.2 W/m^2 were assessed to be, on average, supplied and transferred to the surface, respectively. Thus, an actual heat transfer efficiency of 55 % was computed.

In this perspective, the coupling of hydronic heating systems with energy geostructures emerges as a novel interesting approach to be appropriately investigated. These are ground-contact structures embedding heat exchanger pipes within which the circulation of a heat carrier fluid, usually water or water-glycol mixtures, allows the extraction or the injection of heat from or into the surrounding ground [25,26]. Thus, low-enthalpy geothermal systems are created with tighter land consumption and lesser raw material use with respect to more common vertical borehole heat exchangers. Among them, because of the paramount importance that tunnels have in the development and management of motorway networks [27], energy tunnels [28,29] may embody an excellent source of heat for anti/de-icing purposes. Among a few others, this topic was faced by Baralis et al. [30] and De Feudis et al. [31] with a numerical approach to investigate the feasibility of free-heating systems for, respectively, bridge decks and motorway pavements supplied by energy tunnels nearby.

This paper investigates from the numerical point of view the performance of a hydronic heated pavement supplied by an energy tunnel as a function of geometrical, operational and environmental factors. Thermo-hydraulic numerical analyses are adopted to determine the optimum setup for the hydronic-heated pavement to guide the realisation of a full-scale prototype of an anti-icing system in an existing tunnel in the North-West of Italy. Finally, the economic advantages of a wide-scale adoption are disclosed through a payback analysis.

An energy tunnel-based anti-icing system

In the context of the structural rehabilitation of the Olimpia tunnel (located in North-Western Italy along the A26 motorway between Alessandria and Casale Monferrato), a geothermal anti-icing prototype has been designed and is currently under construction thanks to the partnership with *Autostrade per l'Italia S.p.A*. This prototype consists of a thermally activated tunnel lining for geothermal supply and a hydronic heated pavement for heat dissipation. To effectively convey the heat retrieved from the ground, avoiding heat dissipation, the tunnel and the pavement circuits are connected through pre-insulated supply and return manifolds. The system is designed to operate during both winter and summer, facilitating a recharge of the geothermal reservoir during hot periods [31].

The geothermal supply pipe circuit is composed of four parallel 250.0 m long heat exchanger pipe coils (20.0 × 2.0 mm) clamped on the tunnel wall with a 40.0 cm spacing, following one of the energy retrofitting solutions developed by De Feudis et al. [32]. Accordingly, pipes were arranged after the partial demolition of the existing lining and before the installation of the waterproofing sheeting, as shown in Fig. 1a. This leads to two main advantages.

- The newly built intrados shell is hydraulically isolated from the geothermal coils, thus more easily addressing potential, though unlikely, malfunctioning of the system.
- The geothermal coils are less affected by the enclosed underground environment thanks to the insulation feature of the waterproofing sheeting [32–34].

Analogously, the heat dissipation pipe circuit consists of four parallel 60.0 m long heat exchanger pipe coils (20.0 × 2.0 mm) embedded within the motorway pavement below the wearing and the binder layers, at a depth of approximately 13.0 cm, with a 30.0 cm spacing, as depicted in Fig. 1b.

The system described above was designed to work in free-heating mode (i.e., without the aid of a ground source heat pump) to prevent hoar frost formation on the motorway surface (i.e., snow melting goes beyond the purposes of this specific application). This activates automatically, based on the monitoring outcomes of six temperature probes arranged within the wearing layer. Whenever the road surface temperature falls below 3.0 °C, a smart hydraulic pump is put into operation, thus transferring heat from the ground surrounding the tunnel to the pavement.

The installation of the prototype is more precisely described in De Feudis et al. [36].

Numerical model setup

The optimum heat exchanger pipe geometrical layout for the hydronic heated pavement to be installed at the site (see Fig. 1) was preliminarily identified through thermo-hydraulic numerical analyses using the finite element code FEFLOW© ver. 7.5 [37]. The goal was to aid in the design of the experimental installation currently under construction. Its performance was investigated towards different operational setups and environmental conditions, in order to define appropriate working ranges for the system. The numerical model adopted and the theoretical framework utilised are described in the following.

Problem geometry and material properties

The 3D thermo-hydraulic finite element model developed for this study is depicted in Fig. 2 and counts 322,608 nodes and 611,800 triangular prismatic elements arranged in a 39.0 × 16.5 × 39.0 m domain, enough to ensure no boundary effects. This model aims at reproducing the functioning of a 6.5 × 6.0 m hydronic heated pavement located at the centre of its upper boundary, as shown in Fig. 2. The structural composition of the pavement included 5.0 cm of wearing layer, 5.0 cm of binder layer, 25.0 cm of base layer, 25.0 cm of subbase

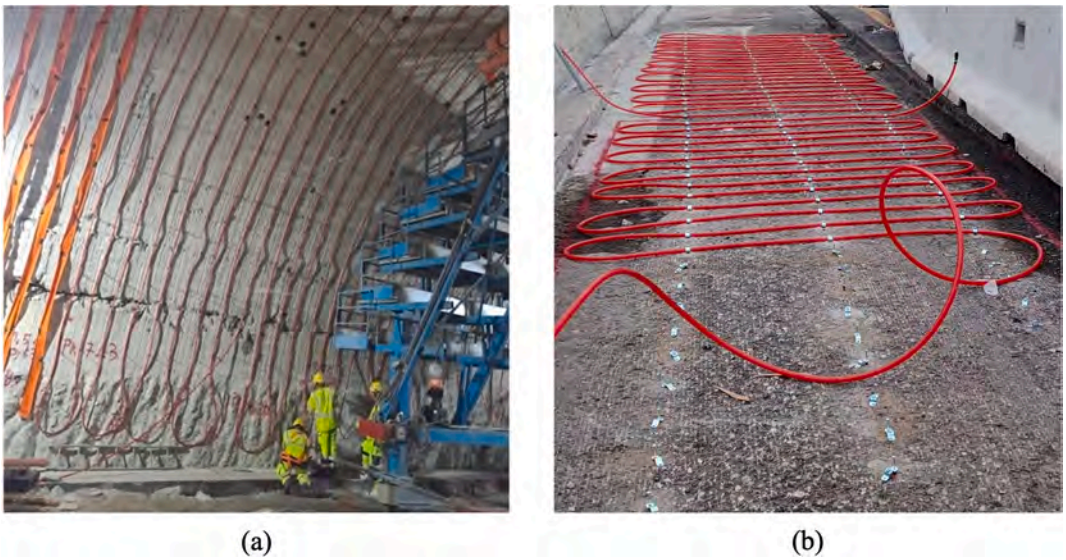

Fig. 1. Heat exchanger pipe setup for the a) geothermal supply [35] and b) heat dissipation circuits.

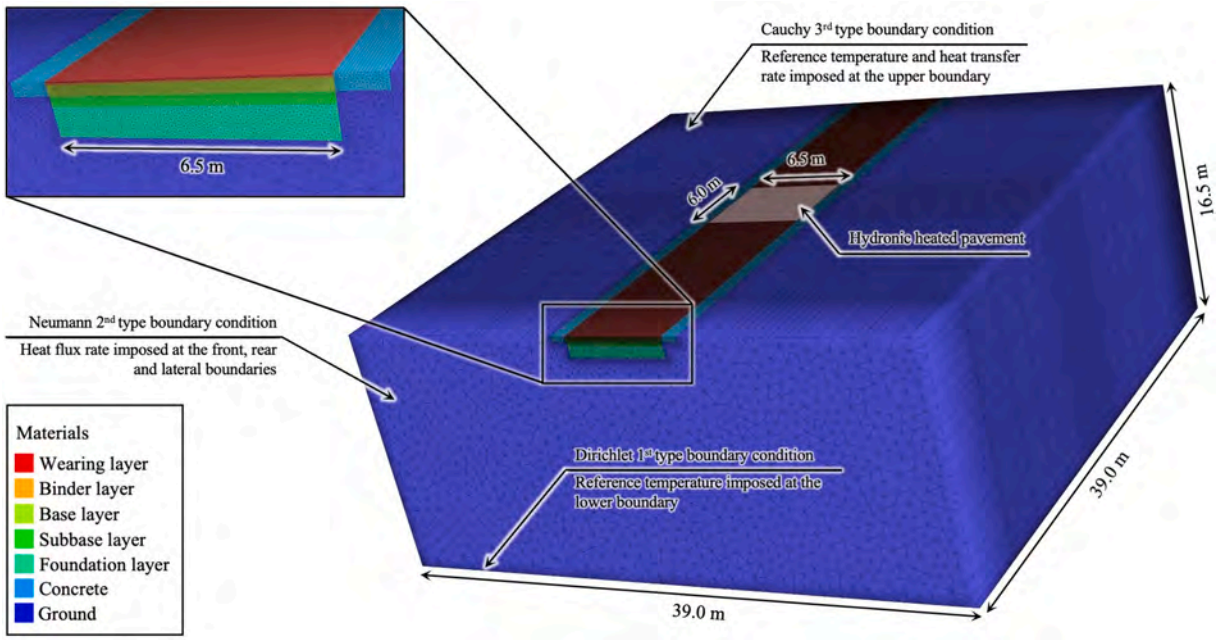

Fig. 2. Sketch of the numerical model geometry and boundary conditions.

layer and 75.0 cm of foundation layer. At the sides of the pavement, two 1.0 m large concrete sidewalks were reproduced. Consistent with the hydrogeological context of the site, the ground underlying the road structure was modelled based on the assumption of completely dry conditions. The thermal properties of the road layers, selected according to Mirzanamedi et al. [38], and the other materials involved in the calculations are listed in Table 1. In line with the hydrogeological setting outlined above, the ground thermal properties are conservatively based on a fixed and null level of saturation.

Table 1
Thermal properties of the materials involved in the numerical calculations.

Materials	Thermal conductivity [W/(mK)]	Thermal capacity [MJ/(m^{3}K)]
Wearing layer	2.24	2.05
Binder layer	1.51	2.31
Base layer	1.44	2.10
Subbase layer	0.70	1.53
Foundation layer	0.80	1.26
Concrete	1.12	2.19
Ground	1.96	1.40
Anti-freezing fluid	0.42	3.94

The heat exchanger pipes within the hydronic heated pavement were reproduced through 1D elements, whose mathematical formulation is discussed in the next Subsection. Different piping layouts, which are illustrated in Fig. 3, were investigated based on the pipe spacing and depth, in the ranges 10.0–60.0 cm and 7.5–22.5 cm, respectively. For each setup, heat exchanger pipes with a cross-section of 201.0 mm^2, corresponding to an external diameter of 20.0 mm and a thickness of 2.0 mm, were considered. Within them, an anti-freezing fluid of propylene-glycol 30 % v/v in water was accounted for, enabling operation at temperatures as low as −10.0 °C.

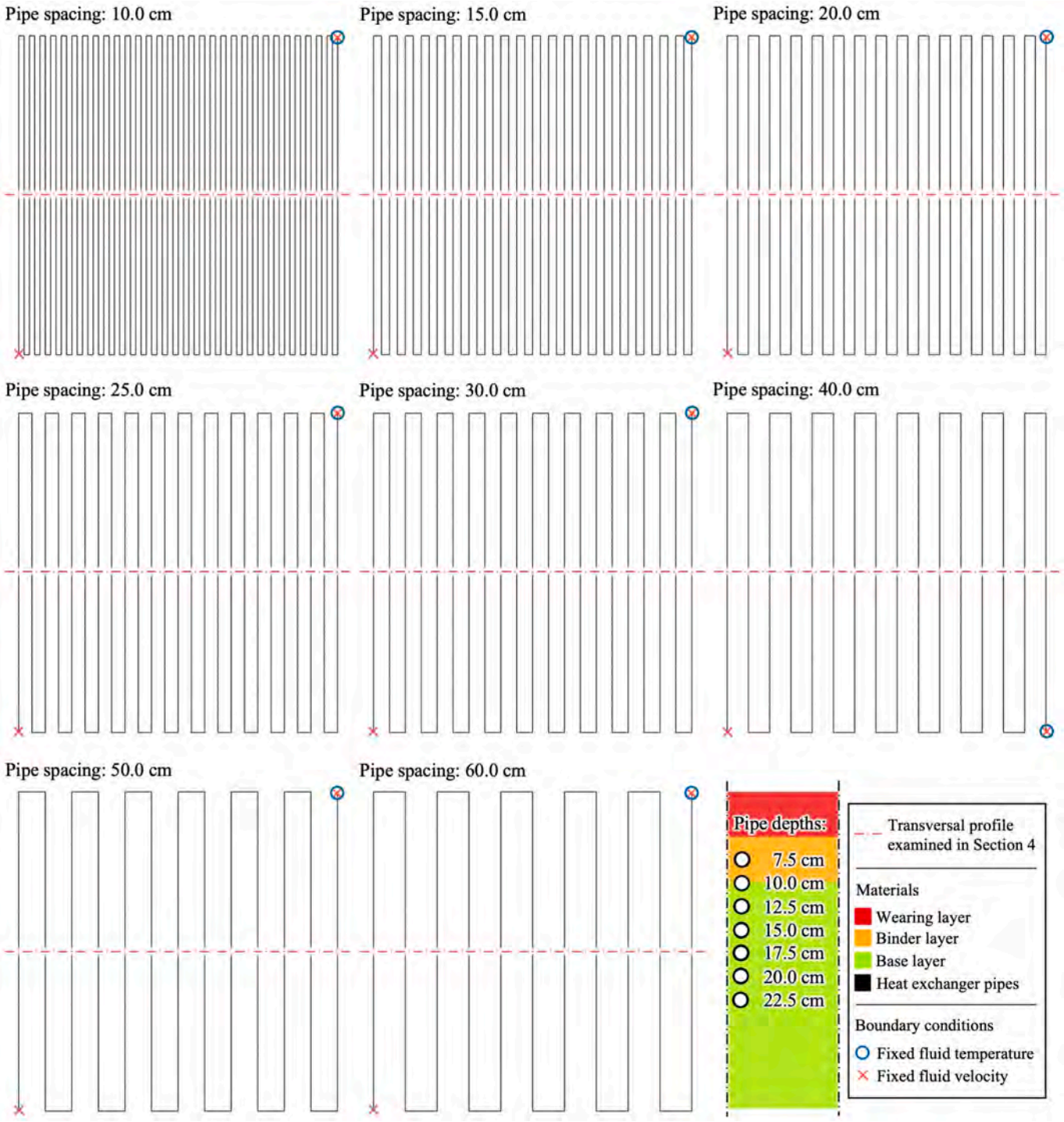

Fig. 3. Heat exchanger pipe geometrical setups simulated in the numerical model as a function of spacing and depth.

Theoretical framework and governing equations

The thermo-hydraulic problem is governed by the theoretical framework presented below which reflects, in a proper reduced form, the complete formulation provided by Diersch [39] for the finite element code FEFLOW©.

Mass balance equation

The mass balance equation governing the flow of the heat carrier fluid within the heat exchanger pipes, under the assumption that thermal expansion has a negligible effect on fluid dynamics, can be articulated as follows:

$$S\frac{\partial p_l}{\partial t} + \nabla \bullet (\rho_l \boldsymbol{v}_l) = 0 \tag{1}$$

where S [1/Pa] indicates the specific storage coefficient; p_l [Pa] is the pressure of the liquid phase; ρ_l [kg/m^3] is the density of the liquid phase; and $\boldsymbol{v}_l$ [m/s] is the velocity vector of the liquid phase.

The fluid flow inside the pipes is reproduced according to the Hagen-Poiseuille's law, which assumes that the fluid particles move in pure translation with a constant velocity along the axial direction $\hat{z}$ of the 1D element:

$$v_{l,\hat{z}} = -\frac{r_{hyd}}{2\mu_l}\left[\frac{\partial p_l}{\partial \hat{z}} - \rho_l g_{\hat{z}}\right] = 0 \quad (2)$$

where $v_{l,\hat{z}}$ [m/s] indicates the liquid phase velocity along the $\hat{z}$ direction; r_{hyd} [m] is the hydraulic radius of 1D element defined as the ratio between the flow area and the wetted perimeter of the fluid; μ_l [Pas] is the dynamic viscosity of the liquid phase; ρ_l [kg/m^3] indicates the density of the liquid phase; and $g_{\hat{z}}$ [m/s] is the gravity component along the $\hat{z}$ direction.

Despite neglecting the thermal resistance due to the pipe wall and fluid regime, these special finite 1D elements were successfully validated for simulating geothermal systems, showing good agreement when compared to analytical solutions [40].

Energy balance equation

The energy balance equation describing the heat exchange throughout the entire domain, under the assumption of negligible thermal inertia of the gas phase and absence of phase change, can be written as follows, with Eq. (3) describing heat transfer in the solid phase and Eq. (4) addressing the same phenomenon in the heat carrier fluid within the heat exchanger pipes:

$$\frac{\partial}{\partial t}[\rho_s c_s T] + \nabla \bullet (\boldsymbol{q}^{cnd}) = Q \quad (3)$$

$$\frac{\partial}{\partial t}[\rho_l c_l T] + \nabla \bullet (\boldsymbol{q}^{cnd} + \boldsymbol{q}^{adv}) = Q \quad (4)$$

where ρ_s [kg/m^3] indicates the density of the solid phase; c_s and c_l [J/(kgK)] are the heat capacities of the solid and liquid phases; T [°C] is the temperature; $\boldsymbol{q}^{cnd}$ and $\boldsymbol{q}^{adv}$ [W/m^2] exemplify the heat exchanged through conduction and advection, respectively; and Q [W/m^3] is the source/sink term.

The amount of heat exchanged by means of conduction (i.e., the transport of heat by diffusion from the more to the less energetic particles of one or more substances due to a combination of their vibration and collision) is quantified through the Fourier's law:

$$\boldsymbol{q}^{cnd} = -\lambda_{i,j}\nabla T \quad (5)$$

where $\lambda_{i,j}$ [W/(mK)] is the thermal conductivity tensor, which, neglecting the contribution of the gas phase, is given by Eq. (6) for use in Eq. (3) and by Eq. (7) for use in Eq. (4):

$$\lambda_{i,j} = \lambda_s \delta_{i,j} \quad (6)$$

$$\lambda_{i,j} = \lambda_l \delta_{i,j} \quad (7)$$

where, λ_s and λ_l [W/(mK)] indicate the thermal conductivities of the solid and liquid phases; $\delta_{i,j}$ [-] is the Kronecker delta.

The amount of heat exchanged through advection (i.e., the transport of heat by bulk fluid flow as a function of pressure and temperature differences within the fluid phase), instead, is quantified as:

$$\boldsymbol{q}^{adv} = \rho_l c_l \boldsymbol{v}_l T \quad (8)$$

The specific governing equations employed in this study accurately mirror the actual hydrogeological context of the site, where there is no groundwater flow and the ground beneath the road structure is entirely dry. As a consequence, while the formulation utilized is thermo-hydraulic in nature, the subsequent discussion will focus exclusively on the thermal aspects of the problem.

Initial and boundary conditions

Sound boundary conditions were chosen to reproduce the thermal behaviour of the hydronic heated pavement (Fig. 2 and Fig. 3). In this regard, the temperature at the lower boundary of the computational domain was forced constant to 12.5 °C through a Dirichlet 1st type thermal boundary condition. It exemplifies the temperature that the ground has beneath the homoeothermic depth [41], which is virtually constant in time and tallies with the annual average temperature of the site at around 10.0–15.0 m depth. Such an assumption is reputed appropriate as the lower boundary of the model deepens below this depth. The same temperature value (i.e., 12.5 °C), used also as initial temperature condition across the entire model domain, is consistent with cold climatic regions, such as the Apennine environment in Italy [32]. In correspondence with the front, rear and lateral boundaries of the numerical model, a Neumann 2nd type thermal boundary condition was used to fix the heat flux there at 0.0 W/m^2.

The numerical analyses aim to test the functionality of the hydronic heated pavement described in Section "An energy tunnel-based anti-icing system". Therefore, a reference ambient air temperature time history was selected based on the recordings of a weather station near the site (see Fig. 4). The harshest time history of the last 5 years was selected, in terms of both the minimum ambient air temperature and the maximum continuous period below 0.0 °C.

The heat transfer between the pavement and the external environment was reproduced through a Cauchy 3rd type thermal boundary condition with a set of heat transfer rates against which the hydronic heated pavement was tested. In the sensitivity analyses carried out, these were varied in the range 2.0–16.0 W/(m^{2}K) to exemplify an increasing convective heat exchange with the external environment. The positive contribution possibly given by solar irradiation was conservatively neglected, considering the road stretch in a shaded area.

The hydronic heated pavement activation was simulated by applying a constant anti-freezing fluid velocity (Neumann 2nd type hydraulic boundary condition) and a constant inlet temperature (Dirichlet 1st type hydraulic boundary condition). Both varied according to proper ranges in the sensitivity analyses, the former within 125–1000 mm/s and the latter within 3.0–9.0 °C. These were selected according to the findings of Baralis et al. [30] and De Feudis et al. [31], who evaluated the feasibility of similar systems working at around 400–500 mm/s and 6.0–6.5 °C of fluid velocity and inlet temperature, respectively.

Model initialisation and the meteorological critical event

The numerical model was preliminarily initialised to get a prospective temperature field for the road pavement before a meteorological critical event was simulated. To this end, a 417-day initialisation was carried out, accounting for the temperature time history mentioned above and the different values of heat transfer rates. As shown in Fig. 4a, the higher the heat transfer rate, and thus the heat exchange with the external environment, the more steadily the pavement reflects the ambient air temperature oscillations. This is even more evident in Fig. 4b, which illustrates the ambient and road pavement temperatures throughout the 11-day meteorological critical event used to test the performance of the hydronic heated pavement.

The selection of this particular 11-day period was purposeful, reflecting extreme yet plausible winter weather conditions that may substantially influence road safety. This timeframe was characterized by sustained sub-zero air temperatures, elevated relative humidity (i.e., an average value along the entire critical period of 90 % with peaks of 98 %), and limited solar radiation (i.e., an average value along the entire critical period of about 150.0 W/m^2 considering the daily time interval 8.00–17.00), conditions that collectively increase the likelihood of hoar frost formation on road surfaces. Therefore, this period serves as a robust benchmark for assessing the efficacy of heated pavement in the specified

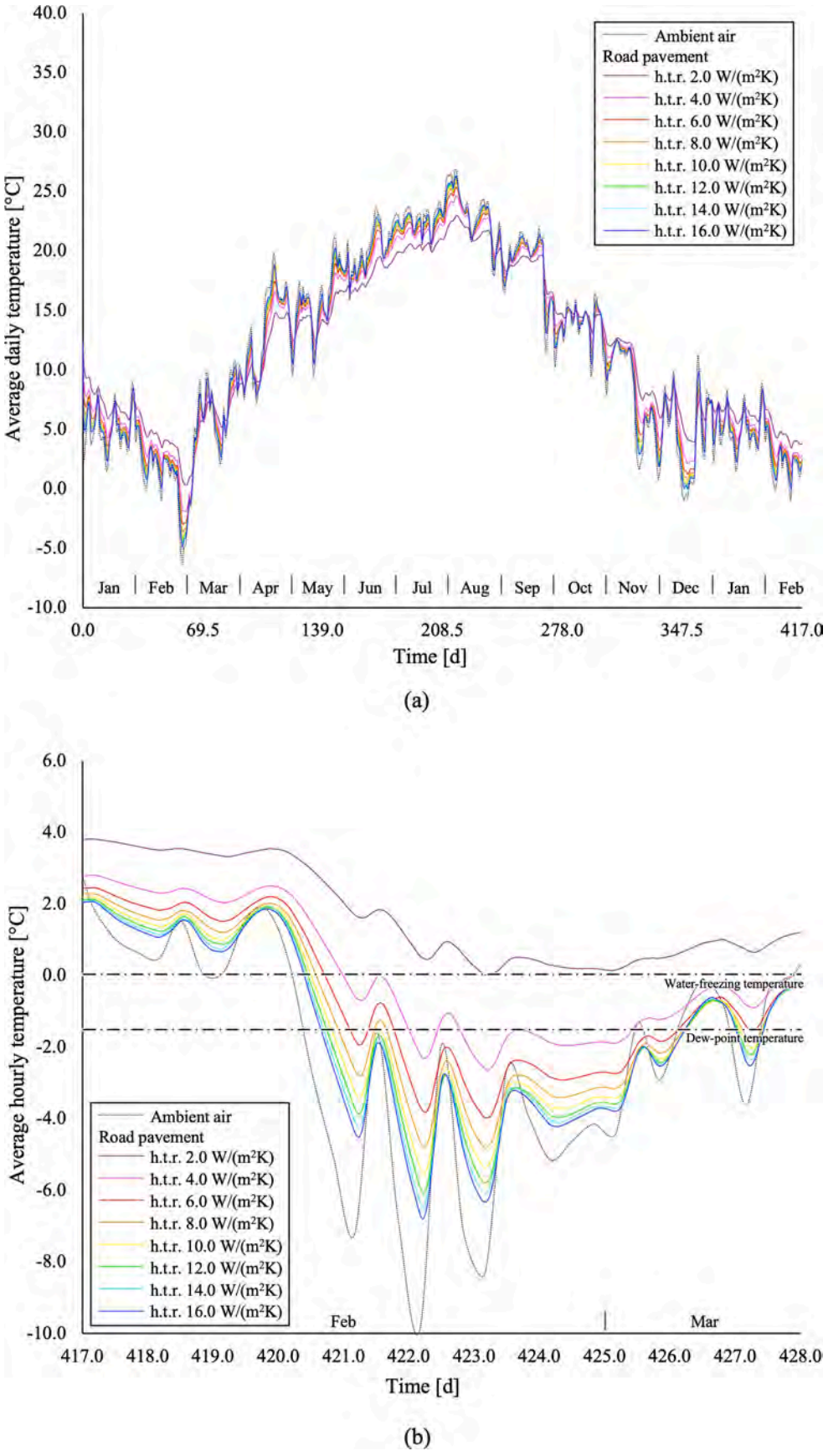

Fig. 4. a) Ambient air temperature time history used for the 417-day model initialisation, b) 11-day meteorological critical event and corresponding behaviour of the road pavement as a function of the heat transfer rate (the abbreviation "h.t.r." refers to "heat transfer rate").

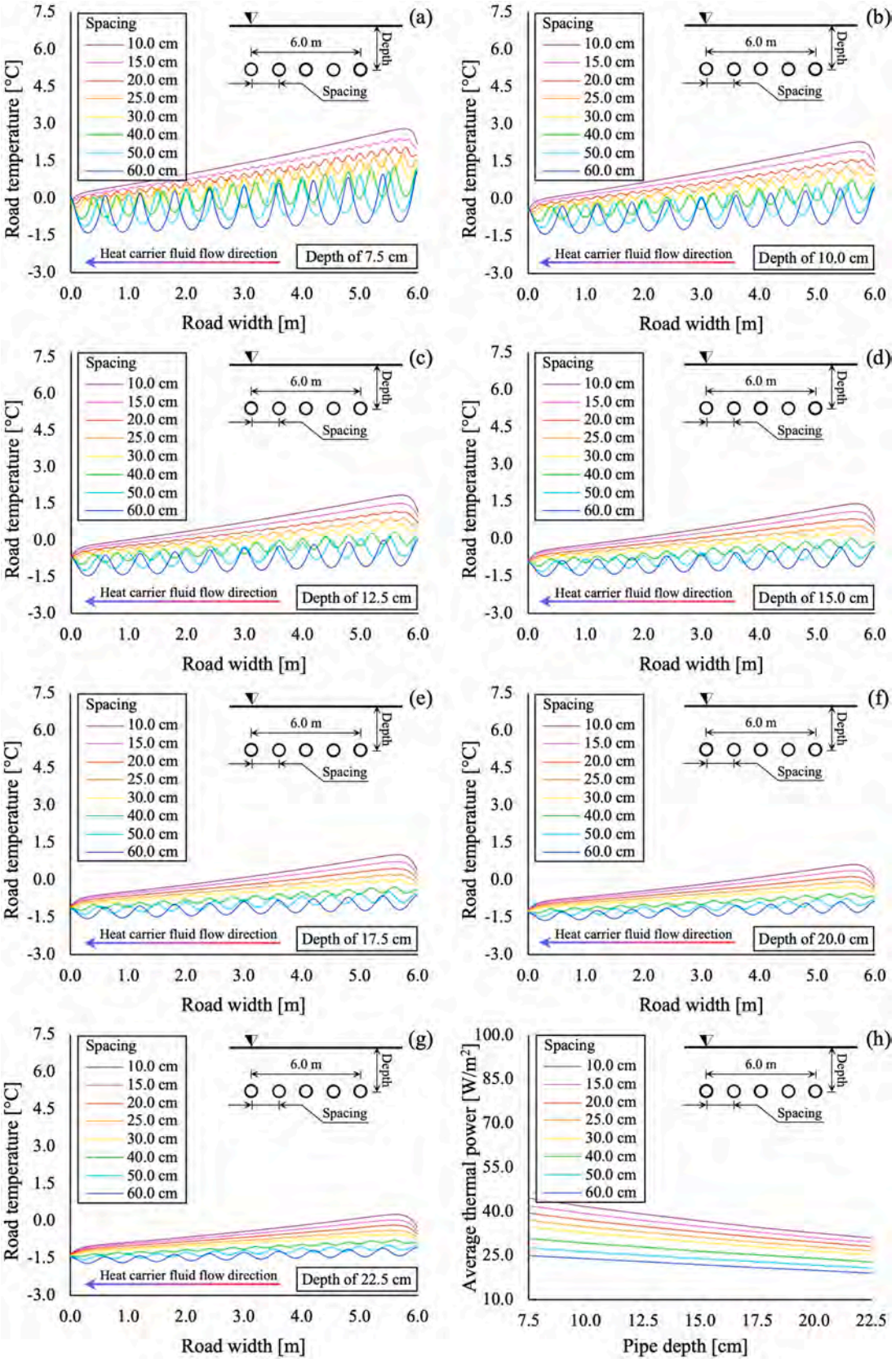

Fig. 5. a-g) Temperature transversal profile along the hydronic heated pavement as a function of the geometrical layout of the pipes, and h) average thermal power released.

climatic region.

During the critical event, as a function of the heat transfer rate, the minimum temperature of the road pavement ranges between 0.2 °C and −7.0 °C for heat transfer rates of 2.0 W/(m^{2}K) and 16.0 W/(m^{2}K), respectively. Accordingly, the slippery period, defined as the cumulative amount of time during which hoar frost formation is assumed to develop, is calculated ranging between 6.9 days to 7.6 days for heat transfer rates of, respectively, 4.0 W/(m^{2}K) and 16.0 W/(m^{2}K), assuming conservatively that hoar frost develops when the road surface temperature drops below 0.0 °C (in the following this condition is referred to as "lower-bound"). Considering, instead, a more realistic situation in which the road freezes when its surface temperature falls below the dew-point temperature, the slippery period is computed as ranging between 3.1 days to 6.0 days for heat transfer rates of, respectively, 4.0 W/(m^{2}K) and 16.0 W/(m^{2}K) and in a scenario in which the amount of absolute water vapour in the air equals 4.4 g/m^3 (90 % relative humidity at 0.0 °C) so that to make the dew-point temperature to reach approximately −1.5 °C (in the following this condition is referred to as "site-specific"). When in the presence of a heat transfer rate of 2.0 W/(m^{2}K), no slippage time was observed even in the absence of hydronic systems. These outcomes will serve as the basis for comparison in the sensitivity analysis results discussed in Section "Sensitivity analysis results".

Sensitivity analysis results

The sensitivity analysis was carried out over the 11-day critical period outlined in the previous section. Because of the free-heating nature of the geothermal anti-icing system, a continuous operation during the whole period was assumed. Free-heating systems, indeed, generally need early activation to counter hoar frost formation effectively. This is because such systems take advantage of the thermal inertia given by a pre-heated road structure rather than large temperature differences within the road surface and the anti-freezing fluid. As previously highlighted in Subsection "Theoretical framework and governing equations", the results discussed in this Section concentrate exclusively on the thermal aspects of the problem.

Influence of the pipe geometrical layout

The influence of the geometrical layout of the heat exchanger pipes (pipe spacing and depth) was evaluated accounting for constant heat carrier fluid inlet temperature and velocity, equal to 6.0 °C and 500 mm/s, respectively, and a standard environmental condition, exemplified by a heat transfer rate of 8.0 W/(m^{2}K). The results obtained are depicted in Fig. 5 in terms of temperature profiles along the hydronic heated pavement taken in the middle of the critical event, together with the average thermal power output during operation.

Fig. 5 shows that as the heat exchanger pipe depth and spacing increase, the average temperature of the road pavement decreases. The same applies to the average thermal power released by the hydronic heated pavement during the test period. Moreover, as the spacing between the pipes increases while maintaining the same depth, the temperature of the road surface becomes progressively wave-shaped across its transversal profile. This is because, on the one hand, narrower-spaced setups predominantly facilitate heat conduction toward the road surface, in contrast to wider-spaced configurations, which tend to exhibit more radial propagation of heat. On the other, the wider the pipe spacing, and, thus, the shorter the pipe layout, the lower the temperature difference experienced by the heat carrier fluid temperature along its path. In this way, the fluid still retains some thermal exchange potential when it reaches the end of the piping circuit. The opposite applies to narrow-spaced pipe setups, which, accordingly, release a larger amount of thermal power, as illustrated in Fig. 5h. It's worth noticing that the temperature peaks formed by wider-spaced pipe setups never match those of narrower-spaced ones. This discrepancy is primarily due to the larger pavement area that needs to be served, which results in the heat dispersing over a wider surface.

The thermal efficiency of the different pipe layouts is computed according to the methodology outlined by Habibzadeh-Bigdarvish et al. [24]. This involves comparing the overall thermal power output against the heat flux that transfers through conduction towards the road surface. The values obtained range between 26 % to 42 %, in agreement with the existing scientific literature [17].

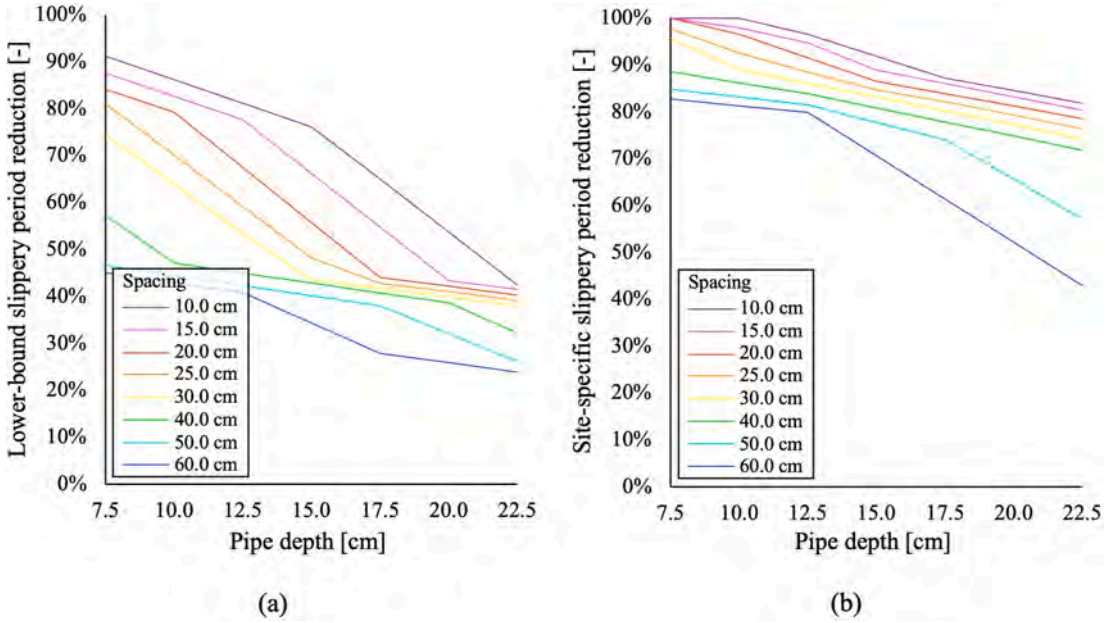

Fig. 6. Slippery period reduction thanks to hydronic heated pavement operation as a function of the geometrical layout of the pipes, considering the a) water freezing temperature (0.0 °C) and b) dew-point temperature (−1.5 °C) as conditions for the development of hoar frost on the pavement surface.

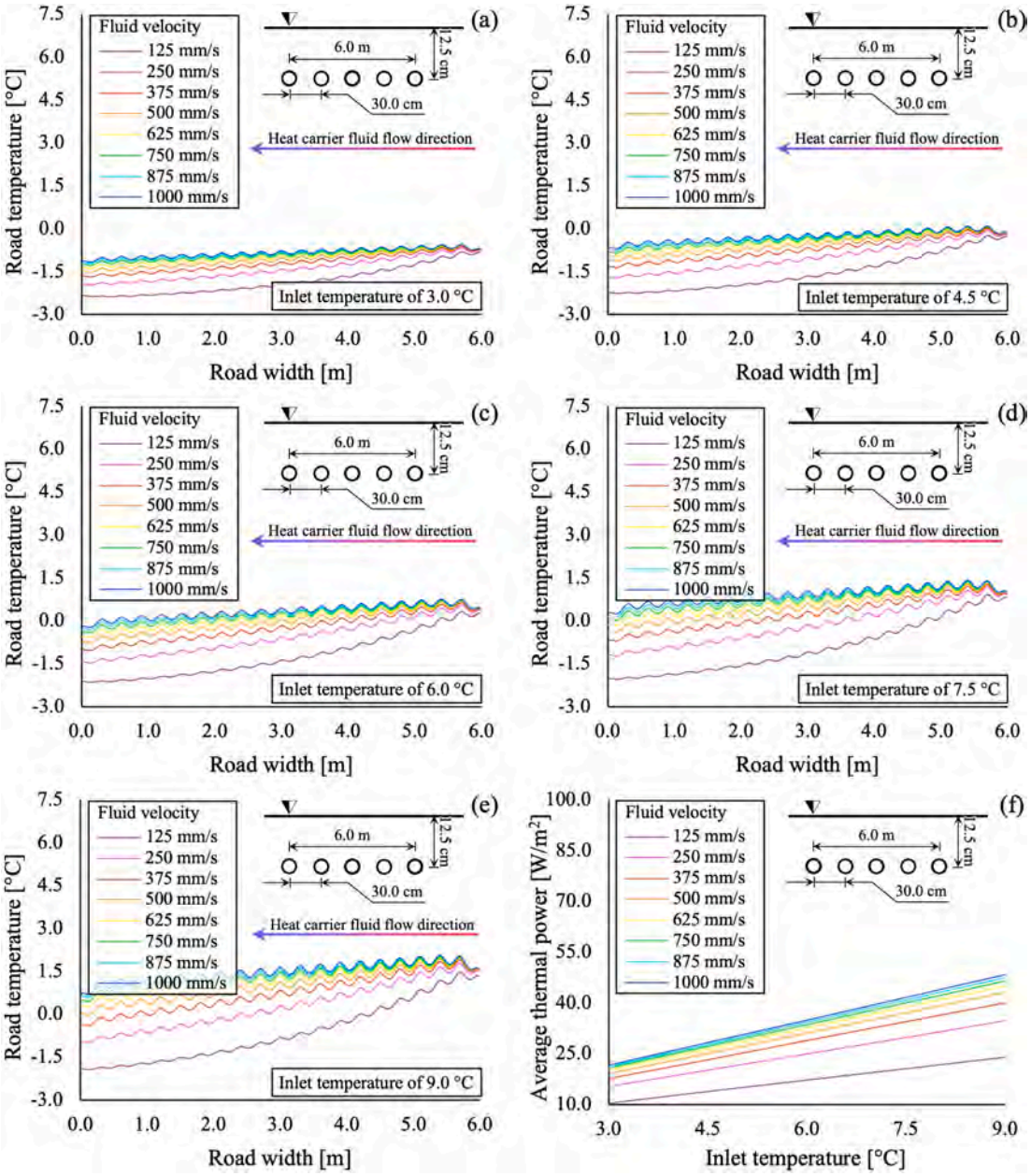

Fig. 7. a-e) Temperature transversal profile along the hydronic heated pavement as a function of the operational setups of the system, and f) average thermal power released.

With the intent to provide a tool for comparison between the different configurations tested, the reduction of the slippery period obtained by activating the hydronic heated pavement, with respect to non-heated pavement (see Subsection "Initial and boundary conditions"), was computed for each geometrical layout. Fig. 6 and Table A1 show the results in percentage for the lower-bound and site-specific hoar frost formation conditions, the latter for the climatic setting described in Subsection "Initial and boundary conditions". These refer to the average temperature of the 6.5 × 6.0 m hydronic heated pavement. It is shown that the system allows for a relevant slippery period reduction, up to 91 % and 100 % for the lower-bound and the site-specific conditions, respectively. The slippery period reduction was found to increase with decreasing both pipe depth and spacing.

From the results illustrated above, the choice towards the shallowest and narrowest pipe layouts may seem straightforward, but it is not. Indeed, the structural integrity of the road pavement should be considered. From this perspective, a deeper piping location reduces the stress peaks and the possibility of crack initiation [42–44]. A compromise must be found between energy and structural aspects. Therefore, it may be advisable to arrange pipes at least beneath the wearing and binder layers. Moreover, narrow-spaced layouts induce large fluid temperature differences, which necessitate being optimised to avoid an anticipated depletion of the geothermal reservoir during the cold season. In this perspective, pipe layouts with spacing ranging between 20.0 cm to 30.0 cm may represent an optimal trade-off, bearing in mind that the more the piping to set up, the higher the costs due to raw materials, labour and pumping. Given all the above, within the results of the sensitivity analysis illustrated in this Subsection (i.e., within a precise and a priori fixed operational and environmental context), an optimised hydronic heated pavement may be able to lower the slippery period by about 75–90 % if the site-specific hoar frost formation criterion is contemplated.

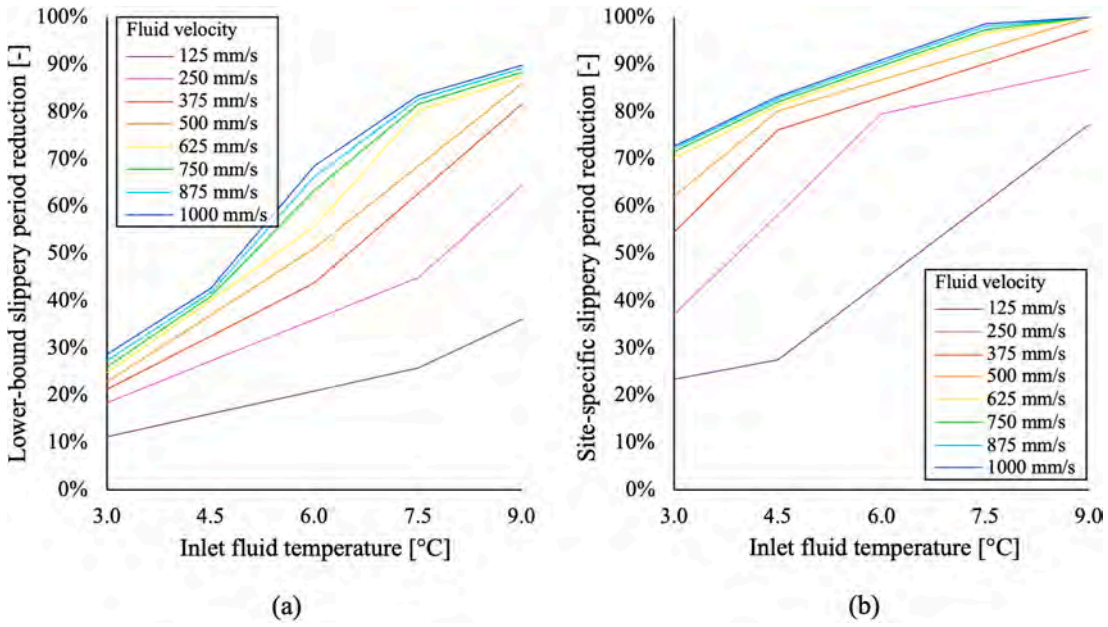

Fig. 8. Slippery period reduction due to hydronic heated pavement operation as a function of the operational setups of the system, considering the a) water freezing temperature (0.0 °C) and b) dew-point temperature (−1.5 °C) as criteria for the development of hoar frost on the pavement surface.

Influence of the operational setups

The influence of the operational setup of the system (velocity and inlet temperature of the fluid) was evaluated accounting for a fixed geometrical layout, corresponding to the piping placed at 12.5 cm depth with a 30.0 cm spacing, and a standard environmental condition, exemplified by a heat transfer rate of 8.0 W/(m^{2}K). The results obtained are depicted in Fig. 7 in terms of temperature profiles along the hydronic heated pavement taken in the middle of the critical event, together with the average thermal power output during operation.

The results shown in Fig. 7 highlight that an increase in the heat carrier fluid inlet temperature or velocity leads to higher road pavement temperatures. This also holds for the average thermal power released by the hydronic heated pavement. It is worth noticing that the colder the inlet temperature of the heat carrier fluid and the slower its velocity, the faster this tends to deplete its thermal exchange potential. This is particularly evident for a velocity of 125 mm/s: depending on the inlet temperature, the heat carrier fluid seems to entirely lose its thermal exchange potential after flowing through from 3.0 m to 5.0 m of road width. Despite inducing the larger fluid temperature difference, slow-flowing setups do not lead to larger thermal discharges. This is because, in the operational context investigated, a given decrease in the fluid velocity leads to an increase in the fluid temperature difference, but never as much to consider the latter effect to prevail over the former, as evident from Fig. 7f.

In this case, thermal efficiencies range between 32 % and 44 % and increase with decreasing fluid inlet temperature and velocity. Despite seeming counterintuitive, this makes sense. On the one hand, the higher the inlet fluid temperature and the larger the amount of heat dissipated towards the deeper layers of the road structure due to the wider temperature unbalance between the fluid and such layers. On the other, as already examined above, lower velocities lead the fluid to deplete its thermal exchange potential earlier, thus preventing heat release towards deeper and warmer road layers.

Fig. 8 and Table A1 show the decrease in the slippery period as a function of the fluid temperature and velocity for the two hoar frost conditions considered. The performance of the system is enhanced by a higher heat carrier fluid inlet temperature and/or velocity due to the larger amount of heat released in the road structure. Considering the water-freezing temperature as rationale for the hoar frost to develop, reductions above 85 % were computed only for operational setups envisaging inlet temperatures of 9.0 °C and velocities as low as 500 mm/

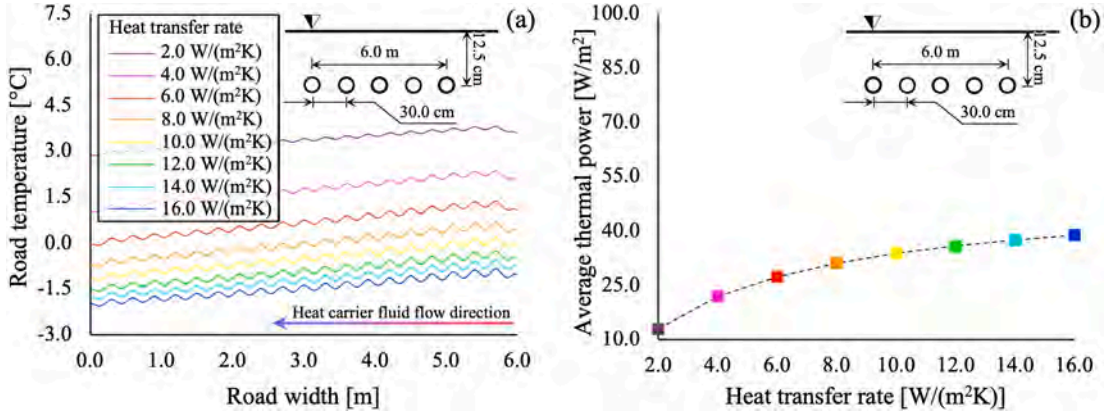

Fig. 9. a) Temperature transversal profile along the hydronic heated pavement as a function of the external environmental conditions and b) average thermal power discharged.

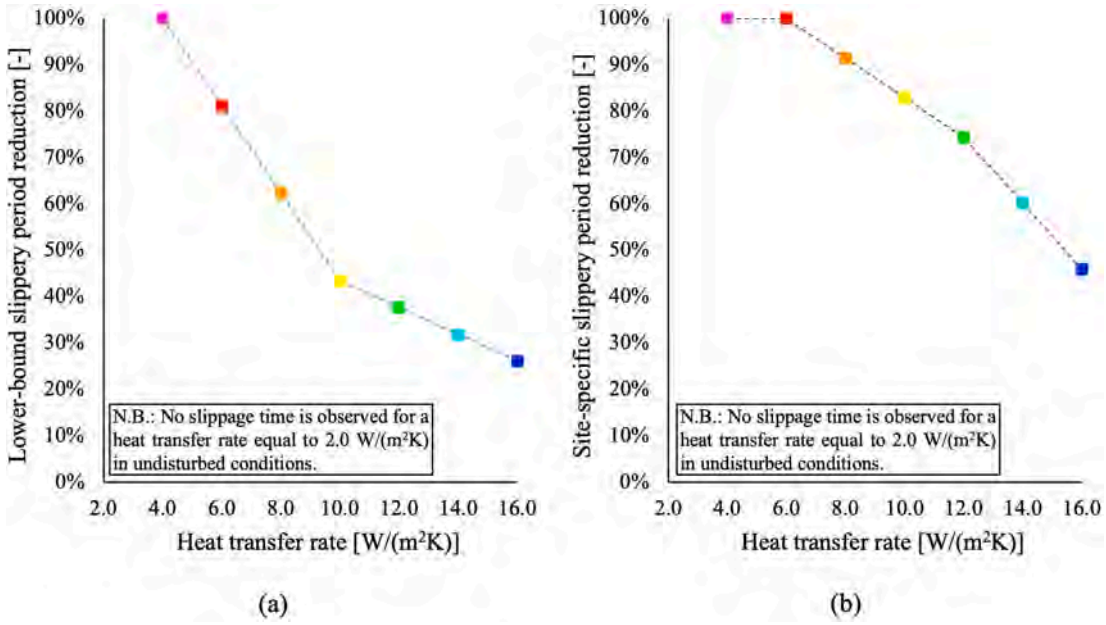

Fig. 10. Slippery period reduction due to hydronic heated pavement operation as a function of the external environmental conditions, considering the a) water freezing temperature (0.0 °C) and b) dew-point temperature (−1.5 °C) as criteria for the development of hoar frost on the pavement surface.

s. Taking into account the dew-point temperature, instead, the same performance was verified for lower inlet temperatures, up to 6.0 °C, and velocities, as low as 250 mm/s.

Despite the performance of such systems improving with the increasing fluid inlet temperatures and velocities, the thermal level of the heat carrier fluid is not manageable for free-heating systems and almost solely depends on the temperature of the geothermal reservoir. Moreover, the faster the heat carrier fluid flows, the higher the operational pumping costs. Indeed, it may be economically and practically onerous to pump such viscous fluids as low-temperature anti-freezing fluids at high velocities. Given all this, it can be advisable to run the geothermal system in the range 375–625 mm/s, depending on the available thermal level of the geothermal reservoir.

Influence of the external environmental conditions

The influence of the environmental conditions of the external environment (heat transfer rate) was measured by contemplating a fixed geometrical layout, corresponding to the piping placed at 12.5 cm depth with a 30.0 cm spacing, and constant heat carrier fluid inlet temperature and velocity, equal to 6.0 °C and 500 mm/s, respectively. The results obtained are depicted in Fig. 9 in terms of temperature profiles along the hydronic heated pavement taken in the middle of the critical event, together with the average thermal power output during operation.

Fig. 9 proves that the harsher the external environment (i.e., the higher the heat transfer rate), the lower the average temperature of the road surface, but the higher the thermal power output. Despite higher amounts of heat released within the pavement structure, this is predominantly dissipated towards the external environment, with percentages of 45 % to 80 %, depending on the harshness of the climate. Obviously, this has an impact on the efficiency of the system in these circumstances, with a negative peak of only around 20 % for a heat transfer rate of 16.0 W/(m^{2}K).

Accordingly, Fig. 10 and Table A1 show that the harsher the external environment, the more difficult it is to accomplish significant non-slippery periods, considering both the water freezing and dew-point

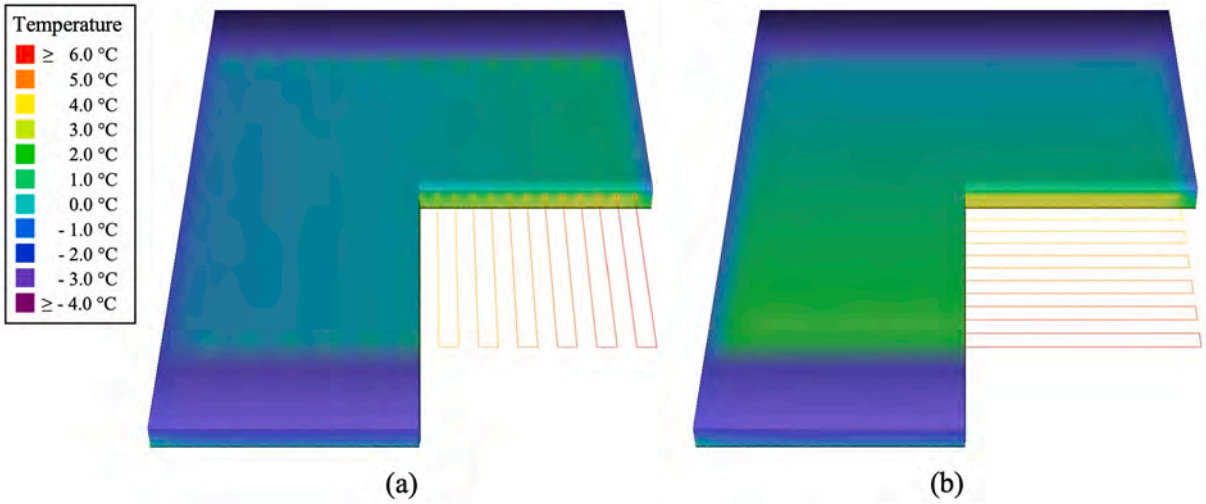

Fig. 11. Temperature fields developed by a) longitudinally and b) transversally arranged heat exchanger pipes on the hydronic heated pavement surface.

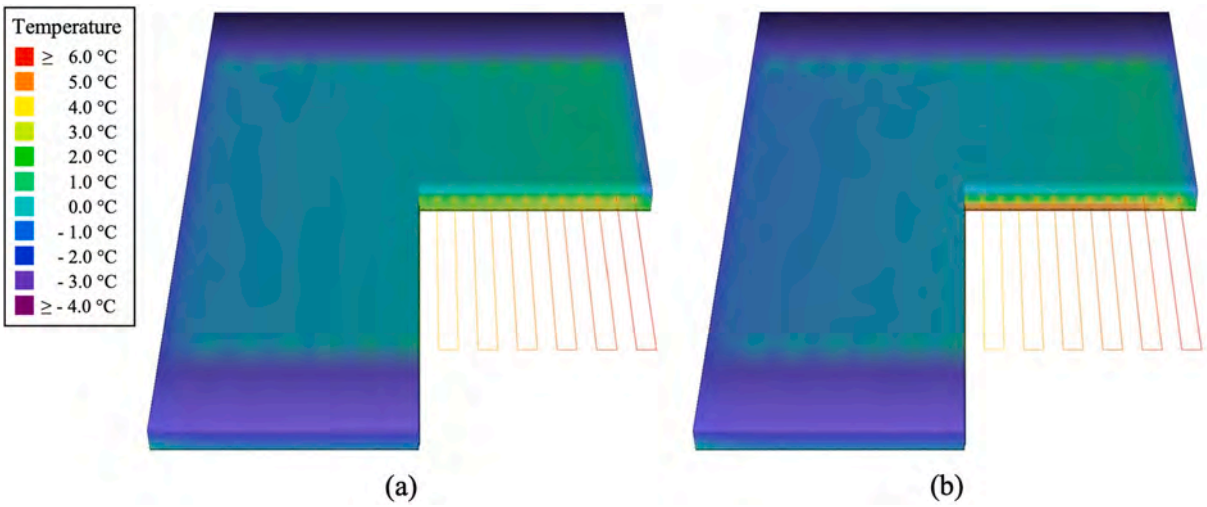

Fig. 12. Temperature fields developed by a) standard and b) XPS-equipped hydronic heated pavements.

temperatures as criteria to initiate hoar frost formation. From this perspective, adjusting the operational setups, which may also be regulated during operation with specific control systems, may be worthwhile to minimise slippage.

Influence of specific design aspects

In this Subsection, two specific design aspects were investigated: the orientation of the heat exchanger pipes and the presence of an insulation layer below the pipe laying plane. For the former purpose, two different layouts were considered to develop temperature gradients along the longitudinal or transversal directions of the road pavement. For the latter aim, an XPS insulation layer was reproduced within the pavement structure, as proposed by Johnsson & Adl-Zarrabi [21,22]. Differently from them, who placed a 10.0 cm thick insulation layer along the interface between the subbase and the foundation layers, this was simulated along the centreline of the base layer (i.e., at a depth of 22.5 cm) with a thickness of 5.0 cm.

Concerning pipe orientation, no significant thermal improvements were found by rotating the pipe layout from longitudinal (Fig. 11a) to transversal (Fig. 11b), as evident from Fig. 11. However, a remarkable aspect arises. Longitudinally arranged pipes develop a thermal gradient, which is transversal to the road width. In very cold periods, this may cause differential slippage between same-axle vehicle wheels, thus posing some degree of risk to driver safety. Conversely, transversal arrangements induce more uniform thermal gradients that evolve longitudinally, which is to be preferred for this field of application.

Regarding the use of XPS, this constitutes a barrier against heat exchange. This means that the temperature of the upper part of the road structure is hardly influenced by its lower portion, which produces the following opposite effects. On the one hand, the XPS layer prevents the heat released within the shallower road layers from being dissipated towards the deeper ones. On the other hand, the former road layers struggle to reach a thermal balance with the latter, thus being, overall, more subjected to the influence of the external environment than solutions not involving insulation. From Fig. 12, which depicts a colder

Fig. 13. A26 motorway stretch from Baveno-Stresa to Brovello-Carpugnino and identification of the icing-prone and the underground motorway portions.

surface temperature for the XPS-equipped hydronic heated pavement, it seems clear that the latter effect prevails over the former, at least in the field of application investigated in this paper.

Indeed, with the same pipe geometrical layout and operational setups, slight improvements in the average power discharged (from 32.9 W/m^2 to 34.4 W/m^2) and the thermal efficiency (from 32 % to 40 %) were noticeable due to the presence of the XPS insulating layer. However, a drop in the slippery period reduction was computed (from 59 % to 49 % for the lower-bound criterion and from 89 % to 85 % for the site-specific one). Provided that structural implications due to the XPS layer embedment within the road structure remain to be investigated, this approach may be reasonable for higher enthalpy applications integrating ground source heat pumps. In this way, the insulating effect of the XPS layer would be exploited properly, thus avoiding dispersing heat towards the deeper portions of the road structure.

Advantages of the wide-scale adoption of energy tunnel-integrated anti-icing systems

The results of the sensitivity analysis, as well as the evidence from real case studies, testify to the functionality of free-heating hydronic heating pavement systems, which undoubtedly represent a flexible and sustainable solution to cope with hoar frost formation on road pavements. Indeed, in contrast to standard de-icing salts spreading machinery, such systems can be automated to activate when needed, thus providing a faster response to adverse climatic conditions.

This Section aims to prove the economic advantages of the wide-scale adoption of energy tunnel based hydronic heating systems for anti-icing purposes. Given the findings arising from Section "Sensitivity analysis results", a hydronic heated pavement characterised by transversally arranged heat exchanger pipes with a depth of 12.5 cm and a spacing of 30.0 cm was taken into account. From the operational point of view, instead, a velocity of the heat carrier fluid of 500 mm/s was opted for. For the sake of this Section, the computations carried out with a heat transfer rate of 8.0 W/(m^{2}K) were accounted for.

The fluid inlet/outlet temperature differences stated by De Feudis et al. [32] for the winter functioning of the same energy retrofitting technology implemented at the Olimpia tunnel (see Section "An energy tunnel-based anti-icing system") were considered to roughly determine the length of the energy tunnel needed to supply the hydronic heating pavement system. In De Feudis et al. [32], these values are the results of 30 days of continuous heat extraction (i.e., three times more than the simulations carried out for the sake of the present research) at a nearly doubled flow rate than that hypothesised here. Consistent with that study, it was assumed that every 3.6 m of energy retrofitted tunnel manages to heat effectively 40.0 m^2 of road pavement.

Given all the above, it was presumed to instrument the 9.0 km long A26 motorway stretch from Baveno-Stresa to Brovello-Carpugnino (both located in the Verbano-Cusio-Ossola province in the Piedmont region, Italy) with energy tunnel based hydronic heating systems. This stretch was identified as perfect for the implementation of the proposed technology since it features around 6.5 km of tunnels with only approximately 32200.0 m^2 of road pavement surface to actively anti-ice, as illustrated in Fig. 13. Indeed, mountainous road stretches like this, characterised by a sequence of tunnels and viaducts or even bridges, perfectly fit the technology described in this research.

Table 2
Input parameters of the payback analysis related to the yearly investment in preventive motorway winter safety using de-icing salts spreading.

Salt trucks usage cost [€/h]	Average salt truck speed [km/h]	Average salt spread [g/m^2]	Average yearly usage [d]	De-icing salt cost [€/ton]
120.0	60.0	25.0	150.0	150.00

Table 3
Input parameters of the payback analysis related to the initial and the running costs for the energy tunnel based hydronic heated system.

PE-Xa pipes [€/m]	Additional workforce [€/m]	Unit head loss for PEX-a pipes [m/km]	Hydraulic pumps cost [€/kW]	Cost of electric energy [€/MWh]
2.50	2.50	80.0	250.00	200.00

To investigate the profitability of the technology, a payback analysis was carried out against the traditional de-icing salt spreading. With this aim, a market analysis was conducted to unveil the yearly amount of money that motorway concessionaires invest to guarantee road safety during cold seasons. By directly interviewing the interested parties (i.e., managers for the winter road safety along specific Italian motorway stretches), it was possible to come up with the input data listed in Table 2. Since the instrumented stretch is significantly shorter than the entire A26 motorway, these are only representative of the preventive winter maintenance, which consists of spreading de-icing salt every night, on average, from mid-October to mid-March. For this reason, Table 2 does not envisage the costs related to machinery annual rental fees or the usage of snowploughs.

Table 3, instead, reports some other input parameters on the energy retrofitting technology from De Feudis et al. [32] used for the payback analysis.

In order to account appropriately for the damage caused by de-icing salt spreading, the study by Dindorf et al. [11] mentioned in Section "Introduction" was taken as a reference. Since this study was carried out later than 10 years ago, those results were qualitatively updated here from 600.0 $/ton to a reasonable value of 1000.0 €/ton. Herein, the effects brought by the loss of purchasing power due to inflation and an increase in the cost of raw materials were conservatively accounted for, as well as the currency exchange.

Given all the above, Fig. 14 proves that the energy tunnel based hydronic heating technology has relatively rapid payback periods ranging from 12 to 15 years. In the latter case, the initial investment was increased by 25 % to account for any possible unforeseen circumstances during construction.

Despite acknowledging that future real large-scale implementations would require more detailed economic analyses (for instance, the Levelized Cost of Energy analysis), such results testify to the attractiveness of the technology, which may be further improved with the implementation of ground source heat pumps. On the one hand, the initial investment and the running annual cost would indeed increase, but on the other, this would allow an enhancement of the functionality of the technology, for instance, making snow melting possible. Apart from the obvious environmental benefits already discussed in Section "Introduction", this would also lead to helpful benefits to motorway customers who, according to Dindorf et al. [11], suffer from $33.0 to $113.0 of vehicle corrosion damages per ton of salt used.

Conclusions

The present paper investigates the performance of energy tunnel based hydronic heated pavement systems. Accordingly, once having outlined some information about the full-scale prototype that is currently under construction, taking advantage of the structural rehabilitation of the Olimpia tunnel (Italy), a sensitivity numerical analysis to investigate the performance of hydronic heated pavements under different pipe geometrical layouts, operational setups, and environmental conditions is carried out. Finally, a payback analysis is performed to prove the attractiveness of the technology.

The following main conclusions can be drawn.

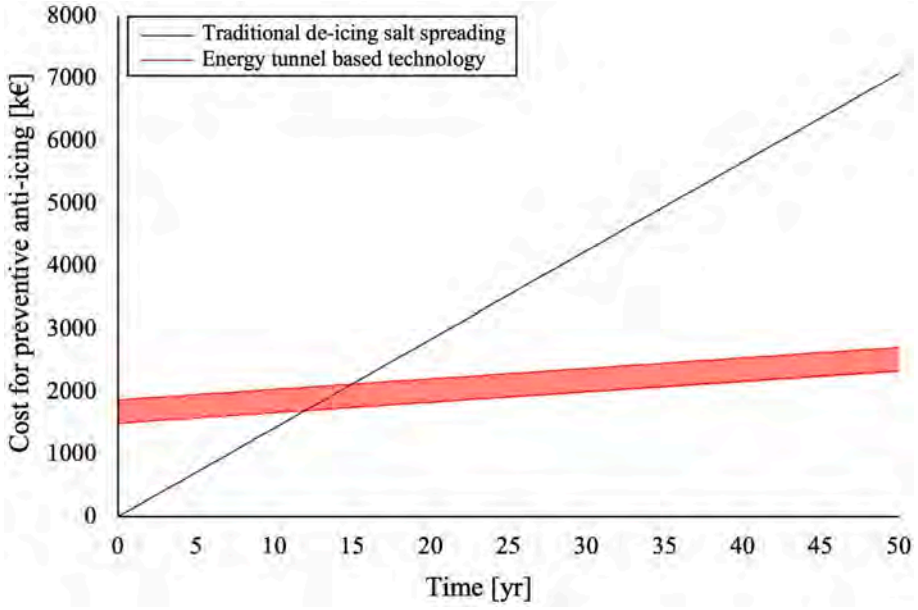

Fig. 14. Cost for preventive anti-icing considering traditional de-icing salt spreading methodology and the proposed energy tunnel-integrated technology.

- Shallower and narrower pipe layouts are not always the optimal layouts. While narrow-spaced layouts induce large fluid temperature differences to be optimised to avoid an anticipated depletion of the geothermal reservoir, shallow ones may jeopardise the structural integrity of the road pavement. A compromise must be found between energy needs and structural integrity. Thus, it may be advisable to arrange pipes at least beneath the wearing and binder layers, optimising the spacing of the serpentine within the range 20.0–30.0 cm.
- Faster heat carrier fluid flows induce undeniable improvements to the heat exchange, but also higher pumping costs. Indeed, it may be economically and practically onerous to pump low-temperature anti-freezing fluids at high velocities. Thus, it can be advisable to run the geothermal system at moderate velocities, based on the available thermal level of the geothermal reservoir, which is not manageable for free-heating systems.
- Considering dew-point temperature, conservatively anyway, instead of water freezing temperature as the threshold value to design hydronic heated pavement may reduce, even significantly, the thermal needs, thus opening doors to free-heating systems to be implemented also in colder regions.
- It may be recommendable to arrange heat exchanger pipes transversally with respect to the longitudinal extension of the road pavement. In this way, a more uniform thermal field is generated on the surface with a thermal gradient following the normal movement of vehicles. XPS-equipped hydronic heated pavements turn out to perform worse than standard ones, at least in the field of application examined.
- Energy tunnel based hydronic heated pavement systems may produce payback periods ranging from 12 to 15 years when applied at a wide scale. The time to recover the cost of the initial investment is expected to reduce with the widening of the application due to the large amount of costs attributable to the rent of the machinery for the entire winter period. These estimates are planned to be furtherly refined in the future, as soon as monitoring data from the Olimpia tunnel experimental site will be available. Large-scale implementations of such a technology would allow to reap the benefits of usage-ready automated geothermal systems aimed at enhancing road safety during cold seasons. Compared to traditional de-icing salt spreading, moreover, this technology embodies a more environment- and infrastructure-friendly solution, which helps reduce environmental impact and enhances infrastructure durability.

Given all the above, the full-scale experimental prototype under construction in the North West of Italy was designed with a geometrical layout of transversally arranged heat exchanger pipes positioned at a depth of about 12.5 cm (i.e., below the wearing and binder layers) and arranged with a spacing of 30.0 cm. Concerning the operational setup, it is envisaged to run the system with heat carrier fluid velocities of 500 mm/s. Moreover, preliminary analyses demonstrated the fluid temperature at the hydronic heated pavement inlet to be about 6.0 °C. In this way, a significant slippery period reduction of about 70 %–90 % can be predicted considering moderate to considerable harshness levels of the external environment.

CRediT authorship contribution statement

S. De Feudis: Writing – review & editing, Writing – original draft, Visualization, Formal analysis, Conceptualization. **A. Insana:** Writing – review & editing, Supervision, Conceptualization. **M. Barla:** Writing – review & editing, Supervision, Funding acquisition, Conceptualization.

Declaration of competing interest

The authors declare that they have no known competing financial interests or personal relationships that could have appeared to influence the work reported in this paper.

Acknowledgements

This study was carried out within the projects “NEST – Network 4 Energy Sustainable Transition” funded under the National Recovery and Resilience Plan (NRRP), Mission 4 Component 2 Investment 1.3 - Call for tender No. 1561 of 11.10.2022 of Ministero dell’Università e della Ricerca and “Georefit – Closing knowledge gaps on energy geostructures for retrofitting of buildings and infrastructures” funded by the Ministero dell’Università e della Ricerca within the PRIN 2022 program (D.D.104

-02/02/2022). This manuscript reflects only the authors' views and opinions and the Ministry cannot be considered responsible for them.

Appendix A

The results of all the numerical analyses performed in terms of the lower-boundary and site-specific slippery period reduction is summarized in Table A1.

Table A1
Results of all the numerical analyses performed (L.B. and S.S. means for "lower-bound" and "site-specific").

Geometrical layout	Constant inlet temperature of 6.0°C, fluid velocity of 500 mm/s and heat transfer rate of 8.0 W/(m²K)							
Pipe depth [cm] \ Pipe spacing [cm]	10.0	15.0	20.0	25.0	30.0	40.0	50.0	60.0
7.5	L.B. 91% S.S. 100%	L.B. 88% S.S. 100%	L.B. 84% S.S. 100%	L.B. 81% S.S. 98%	L.B. 74% S.S. 96%	L.B. 57% S.S. 89%	L.B. 47% S.S. 85%	L.B. 45% S.S. 83%
10.0	L.B. 86% S.S. 100%	L.B. 83% S.S. 98%	L.B. 79% S.S. 97%	L.B. 70% S.S. 93%	L.B. 64% S.S. 89%	L.B. 47% S.S. 86%	L.B. 44% S.S. 83%	L.B. 43% S.S. 81%
12.5	L.B. 81% S.S. 97%	L.B. 78% S.S. 95%	L.B. 68% S.S. 92%	L.B. 59% S.S. 89%	L.B. 53% S.S. 86%	L.B. 45% S.S. 84%	L.B. 42% S.S. 81%	L.B. 41% S.S. 80%
15.0	L.B. 76% S.S. 92%	L.B. 66% S.S. 89%	L.B. 56% S.S. 87%	L.B. 48% S.S. 85%	L.B. 44% S.S. 83%	L.B. 43% S.S. 81%	L.B. 40% S.S. 78%	L.B. 34% S.S. 71%
17.5	L.B. 65% S.S. 87%	L.B. 55% S.S. 86%	L.B. 44% S.S. 84%	L.B. 43% S.S. 82%	L.B. 42% S.S. 80%	L.B. 41% S.S. 78%	L.B. 38% S.S. 74%	L.B. 28% S.S. 61%
20.0	L.B. 54% S.S. 85%	L.B. 43% S.S. 83%	L.B. 42% S.S. 81%	L.B. 41% S.S. 79%	L.B. 40% S.S. 77%	L.B. 39% S.S. 75%	L.B. 32% S.S. 66%	L.B. 26% S.S. 52%
22.5	L.B. 42% S.S. 82%	L.B. 41% S.S. 80%	L.B. 40% S.S. 79%	L.B. 39% S.S. 76%	L.B. 38% S.S. 74%	L.B. 32% S.S. 72%	L.B. 26% S.S. 57%	L.B. 24% S.S. 43%
Operational setup	Constant pipe spacing of 30.0 cm, pipe depth of 12.5 cm and heat transfer rate of 8.0 W/(m²K)							
Inlet temperature [°C] \ Fluid velocity [mm/s]	125	250	375	500	625	750	875	1000
3.0	L.B. 11% S.S. 23%	L.B. 18% S.S. 37%	L.B. 21% S.S. 55%	L.B. 23% S.S. 62%	L.B. 25% S.S. 70%	L.B. 26% S.S. 72%	L.B. 27% S.S. 72%	L.B. 29% S.S. 73%
4.5	L.B. 16% S.S. 28%	L.B. 27% S.S. 58%	L.B. 33% S.S. 76%	L.B. 37% S.S. 80%	L.B. 40% S.S. 81%	L.B. 41% S.S. 82%	L.B. 42% S.S. 83%	L.B. 43% S.S. 83%
6.0	L.B. 21% S.S. 44%	L.B. 36% S.S. 80%	L.B. 44% S.S. 83%	L.B. 51% S.S. 87%	L.B. 56% S.S. 89%	L.B. 63% S.S. 90%	L.B. 66% S.S. 90%	L.B. 68% S.S. 91%
7.5	L.B. 26% S.S. 61%	L.B. 45% S.S. 84%	L.B. 63% S.S. 90%	L.B. 69% S.S. 93%	L.B. 80% S.S. 97%	L.B. 82% S.S. 97%	L.B. 83% S.S. 98%	L.B. 83% S.S. 99%
9.0	L.B. 36% S.S. 77%	L.B. 64% S.S. 89%	L.B. 82% S.S. 97%	L.B. 86% S.S. 100%	L.B. 87% S.S. 100%	L.B. 88% S.S. 100%	L.B. 89% S.S. 100%	L.B. 90% S.S. 100%
Environmental conditions	Constant pipe spacing of 30.0 cm, pipe depth of 12.5 cm, inlet temperature of 6.0°C and fluid velocity of 500 mm/s							
Heat transfer rate [W/(m²K)]	2.0	4.0	6.0	8.0	10.0	12.0	14.0	16.0
-	L.B. - S.S. -	L.B. 100% S.S. 100%	L.B. 81% S.S. 100%	L.B. 61% S.S. 91%	L.B. 43% S.S. 83%	L.B. 38% S.S. 74%	L.B. 32% S.S. 60%	L.B. 26% S.S. 46%
Specific aspects	Constant pipe spacing of 30.0 cm, pipe depth of 12.5 cm, inlet temperature of 6.0°C, fluid velocity of 500 mm/s and heat transfer rate of 8.0 W/(m²K)							
Design aspects	Transversally arranged heat exchanger pipes				XPS-layer embedded along the centreline of the base layer			
-	L.B. 59% S.S. 89%				L.B. 49% S.S. 85%			

Data availability

Data will be made available on request.

References

[1] Zhang J, Das DK, Peterson R. Comprehensive evaluation of bridge anti-icing technologies. 2007.
[2] Fay L, Shi X. Environmental impacts of chemicals for snow and ice control: state of the knowledge. Water Air Soil Pollut 2012;223(5):2751–70. https://doi.org/10.1007/s11270-011-1064-6.
[3] Lee H, Cody RD, Cody aM, Spry PG. Effects of Various Deicing Chemicals on Pavement Concrete Deterioration. Proc Mid-Continent Transp Symp 2000:151–5.
[4] Feng B, Wang H, Li S, Ji K, Li L, Xiong R. The durability of asphalt mixture with the action of salt erosion: a review. Constr Build Mater 2022;315:125749. https://doi.org/10.1016/j.conbuildmat.2021.125749.
[5] Juli-Gándara L, Vega-Zamanillo Á, Calzada-Pérez M. Sodium chloride effect in the mechanical properties of the bituminous mixtures. Cold Reg Sci Technol 2019;164:102776. https://doi.org/10.1016/j.coldregions.2019.05.002.
[6] Juli-Gándara L, Vega-Zamanillo Á, Calzada-Pérez MÁ, Teijón-López-Zuazo E. Effect of sodium chloride on the modulus and fatigue life of bituminous mixtures. Materials 2020;13(9). https://doi.org/10.3390/ma13092126.
[7] Wang F, Qin X, Pang W, Wang W. Performance deterioration of asphalt mixture under chloride salt erosion. Materials 2021;14(12):3339. https://doi.org/10.3390/ma14123339.
[8] Eugster, W. J. (2007). Road and Bridge Heating Using Geothermal Energy, Overview and Examples. European Geothermal Congress, June, 5.
[9] Hintz WD, Fay L, Relyea RA. Road salts, human safety, and the rising salinity of our fresh waters. Front Ecol Environ 2022;20(1):22–30. https://doi.org/10.1002/fee.2433.
[10] Kaushal SS, Likens GE, Pace ML, Utz RM, Haq S, Gorman J, et al. Freshwater salinization syndrome on a continental scale. PNAS 2018;115(4):E574–83. https://doi.org/10.1073/pnas.1711234115.
[11] Dindorf C, Fortin C, Asleson B, Erdmann J. The real cost of salt use for winter maintenance in the twin cities metropolitan area. 2014.
[12] Tuan CY. Roca spur bridge: the implementation of an innovative deicing technology. J Cold Reg Eng 2008;22(1):1–15. https://doi.org/10.1061/(asce)0887-381x(2008)22:1(1).
[13] Yang Z, Yang T, Song G, Singla M. Experimental Study on an Electrical Deicing Technology Utilizing Carbon Fiber Tape. 2012.
[14] Heliasz Z, Ostaficzuk S. How to use waste heat and geothermal energy for de-snowing and De-Icing in Poland - Concepts and problems. Proce Int Scientific Conference Geothermal Energy in Underground Min 2001:149–54. http://kgp.wnoz.us.edu.pl/Pdf/a18.pdf.
[15] Daniels JW, Heymsfield E, Kuss M. Hydronic heated pavement system performance using a solar water heating system with heat pipe evacuated tube solar collectors. Sol Energy 2019;179:343–51. https://doi.org/10.1016/j.solener.2019.01.006.
[16] Eugster WJ, Schatzmann J. Harnessing Solar Energy for Winter Road Clearing on Heavily Loaded Expressways. XI PIARC International Winter Road Congress 2002;9.
[17] Morita K, Tago M. Snow-melting on sidewalks with ground-coupled heat pumps in a heavy snowfall city. Proce World Geothermal Congress 2005;April:24–9.
[18] Islam MS, Fukuhara T, Watanabe H, Nakamura A. Horizontal U-tube road heating system using tunnel ground heat. J Snow Eng Japan 2006;22(3):23–8.
[19] Yoshitake I, Yasumura N, Syobuzako M, Scanlon A. Pipe heating system with underground water tank for snow thawing and ice prevention on roads and bridge decks. J Cold Reg Eng 2011;25(2):71–86. https://doi.org/10.1061/(asce)cr.1943-5495.0000023.
[20] Barbagallo D. RPD 155 Heated Pavements. 2013.
[21] Johnsson J, Adl-Zarrabi B. Modeling the thermal performance of low temperature hydronic heated pavements. Cold Reg Sci Technol 2019;161(February):81–90. https://doi.org/10.1016/j.coldregions.2019.03.007.
[22] Johnsson J, Adl-Zarrabi B. A numerical and experimental study of a pavement solar collector for the northern hemisphere. Appl Energy 2020;260:114286. https://doi.org/10.1016/j.apenergy.2019.114286.
[23] Ou T, Hu Y, Gustavsson T, Bogren J. On the relationship between the risk of hoar frost on roads and a changing climate in Sweden. Int J Climatol 2019;39(5):2601–11. https://doi.org/10.1002/joc.5974.
[24] Habibzadeh-Bigdarvish O, Yu X, Li T, Lei G, Banerjee A, Puppala AJ. A novel full-scale external geothermal heating system for bridge deck de-icing. Appl Therm Eng 2021;185:116365. https://doi.org/10.1016/j.applthermaleng.2020.116365.
[25] Brandl H. Energy foundations and other thermo-active ground structures. Geotechnique 2006;56(2):81–122. https://doi.org/10.1680/geot.2006.56.2.81.
[26] Laloui, L., & Di Donna, A. (2013). *Energy* Geostructures: Innovation in Underground Engineering. John Wiley & Sons, 2013.
[27] De Feudis S, Insana A, Barla M. A simple parametric numerical model to assist the design of repair works and maintenance of tunnels. Springer Series in Geomechanics and Geoengineering 2023:654–61. https://doi.org/10.1007/978-3-031-34761-0_79.
[28] Adam D, Markiewicz R. Energy from earth-coupled structures, foundations, tunnels and sewers. Geotechnique 2009;59(3):229–36. https://doi.org/10.1680/geot.2009.59.3.229.
[29] Barla M, Di Donna A, Insana A. A novel real-scale experimental prototype of energy tunnel. Tunn Undergr Space Technol 2019;87(January):1–14. https://doi.org/10.1016/j.tust.2019.01.024.
[30] Baralis M, Insana A, Barla M. Energy tunnels for deicing of a bridge deck in alpine region. Lecture Notes in Civil Eng 2021;126:1061–8. https://doi.org/10.1007/978-3-030-64518-2_126.
[31] De Feudis S, Insana A, Barla M. Sfruttamento geotermico di gallerie esistenti a fini di anti-icing stradale. Incontro Annuale Dei Giovani Ingegneri Geotecnici 2024:33–6.
[32] De Feudis S, Insana A, Barla M. Seizing the opportunity of energy retrofitting of existing tunnels. Tunn Undergr Space Technol 2024;154:106109. https://doi.org/10.1016/j.tust.2024.106109.
[33] Lee C, Park S, Won J, Jeoung J, Sohn B, Choi H. Evaluation of thermal performance of energy textile installed in Tunnel. Renew Energy 2012;42:11–22. https://doi.org/10.1016/j.renene.2011.09.031.
[34] Lee C, Park S, Choi HJ, Lee IM, Choi H. Development of energy textile to use geothermal energy in tunnels. Tunn Undergr Space Technol 2016;59:105–13. https://doi.org/10.1016/j.tust.2016.06.014.
[35] Barla, M., Cecinato, F., Salciarini, D., Sterpi, D., Alvi, M. R., Angelotti, A., Capati, G., De Feudis, S., Gerola, M., Insana, A., Lupattelli, A., Morcioni, A., Rafai, M., & Scerbo, M. (2025). Utilizzo delle geostrutture energetiche per il retrofitting di edifici e infrastrutture. *XXVIII Convegno Nazionale Di Geotecnica*.
[36] De Feudis, S., Insana, A., & Barla, M. (2025). The first worldwide energy-retrofitted tunnel.
[37] DHI. Feflow 7.5 – Finite element simulation system for subsurface flow & transport processes. Berlin: DHI-WASY GmbH; 2022.
[38] Mirzanamadi R, Hagentoft C-E, Johansson P. Numerical Investigation of Anti-Icing Road Surfaces using Hydronic Heating Pavement- Parametric Study. In: 16th IBPSA International Conference and Exhibition, 2008; 2019. p. 524–31. https://doi.org/10.26868/25222708.2019.211126.
[39] Diersch HJG. FEFLOW: Finite Element Modeling of Flow, Mass and Heat Transport in Porous and Fractured Media. Berlin: Springer-Verlag; 2014. p. 996.
[40] Diersch HJG. DHI-WASY software – Feflow 6.1 – Finite element subsurface flow & transport simulation system: reference manual. Berlin: DHI-WASY GmbH; 2009.
[41] Barbero D, De Luca DA, Forno MG, Lasagna M. Preliminary results on temperature distribution in the Quaternary fluvial and outwash deposits of the Piedmont Po Plain (NW Italy): a statistical approach. Rendiconti Online Societa Geologica Italiana 2016;41:272–5. https://doi.org/10.3301/ROL.2016.146.
[42] Ghalandari T, Kia A, Taborda DM, Vuye C. Thermal and structural response of a pavement solar collector prototype. Symposium on Energy Geotechnics. 2023:5–6. https://doi.org/10.59490/seg.2023.511.
[43] Ghalandari T, Hernando D, Omranian SR, Van Den Bergh W, Vuye C. Mechanical response assessment of pavement solar collectors. Bituminous Mixtures and Pavements VIII 2024;408–414. https://doi.org/10.1201/9781003402541-48.
[44] van Bijsterveld WT, Houben LJM, Scarpas A, Molenaar AAA. Using pavement as solar collector. Transp Res Rec 2001;1778:140–8.